JACS
JOURNAL OF THE AMERICAN CHEMICAL SOCIETY

Article

pubs.acs.org/JACS

Molybdenum Carbide Nanocatalysts at Work in the in Situ Environment: A Density Functional Tight-Binding and Quantum Mechanical/Molecular Mechanical Study

Xingchen Liu and Dennis R. Salahub*

Department of Chemistry, Institute for Quantum Science and Technology, and Centre for Molecular Simulation, University of Calgary, 2500 University Drive NW, Calgary, Alberta T2N 1N4, Canada

Supporting Information

ABSTRACT: Heterogeneous reactions catalyzed by transition-metal-containing nanoparticles represent a crucial type of reaction in chemical industry. Because of the existing gap in understanding heterogeneous catalysis between a cluster of a few atoms and a bulk model of periodic slabs, reactions catalyzed by transition-metal-containing nanoparticles are still not well understood. Herein, we provide a multiscale modeling approach to study the benzene hydrogenation reactions on molybdenum carbide nanoparticles (MCNPs) in the process of in situ heavy oil upgrading. By coupling the quantum mechanical (QM) density functional tight-binding (DFTB) method with a molecular mechanical (MM) force field, a QM/MM model was built to describe the reactants, the nanoparticles and the surroundings. Umbrella sampling (US) was used to calculate the free energy profiles of the benzene hydrogenation reactions in a model aromatic solvent in the in situ heavy oil upgrading conditions. By comparing with the traditional method in computational heterogeneous catalysis, the results reveal new features of the metallic MCNPs. Rather than being rigid, they are very flexible under working condition due to the entropic contributions of the MCNPs and the solvent, which greatly affect the free energy profiles of these nanoscale heterogeneous reactions.

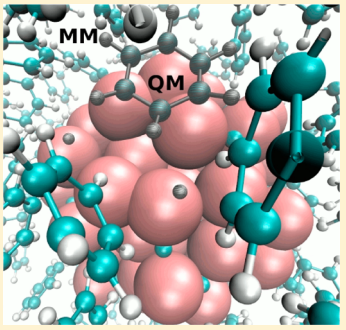

INTRODUCTION

Nanocatalysts, usually considered as heterogeneous catalysts, are long-established in industry due to their unique properties compared with those of the same materials in bulk form. In the petrochemical industry, for example, molybdenum carbide nanoparticles (MCNPs) were found to have high activity in the conversion of heavy oil and tar sands into lighter hydrocarbons.[1] Not only can they be used in the refinery, they can also be injected into oil reservoirs for underground prerefining to help the upgrading of heavy oil, which is also called "in situ catalysis".[2,3]

In heterogeneous catalysis, the catalyst is usually modeled by either a small cluster of a few tens of atoms or by a periodic slab. Along these lines, we have previously reported first-principles electronic structure calculations on both the $Mo_{38}C_{19}$ cluster[4] and the bulk.[5] All of these studies, however, may have missed some important features of the reactions on MCNPs. First, neither the small cluster nor the periodic studies could reflect the correct local topology of the active sites on the MCNPs;[6] both of them used flat surfaces cut from the bulk structure. However, it is known that adsorption is a local phenomenon, and the active site topology may greatly affect the way the adsorbents interact with the catalyst and their mobility, modifying the overall energy profiles. Second, neither of these methods could describe the electronic structural characteristics of the MCNPs: the delocalization of electron density over the entire nanoparticle. A cluster of tens of atoms is too small, while the periodic model ignores quantum size effects. Third, because of the complexity of the surface morphologies of the MCNPs, there may be many local minima for the attacking H to adsorb on the potential energy surface. It is very difficult to find the proper reactant site on the MCNPs. Fourthly, and most importantly, traditional methods usually calculate the energy of the stationary points in the gas phase, while the environment and the temperature (entropic effects) are often ignored, or sometimes treated within a harmonic oscillator approximation.

With the motivation of improving on the traditional approach, in this work, we present a multiscale modeling approach to study the MCNP-catalyzed hydrogenation reactions under working conditions. We first use a semi-empirical quantum chemical (QM) density functional tight-binding (DFTB)[7−9] approach to calculate the potential energy surfaces for benzene hydrogenation on three MCNPs of different sizes, 1.2, 1.9, and 2.3 nm in the gas phase, generating a traditional "picture" of the reactions with potential energy surfaces. Then in our improved approach, the smaller 1.2 nm MCNP was embedded into a solvent environment of 100 benzene molecules. Using a combined quantum mechanical and molecular mechanical (QM/MM)[10] method and the umbrella sampling[11] (US) technique, the free energy profiles of benzene hydrogenation on the MCNP at 673 K in the model aromatic environment are calculated. With this multiscale

Received: February 10, 2015
Published: March 16, 2015

DOI: 10.1021/jacs.5b01494
J. Am. Chem. Soc. 2015, 137, 4249−4259

method, we were able to get a better picture of the benzene hydrogenation reaction on MCNPs in the in situ environment.

COMPUTATIONAL METHODS

QM Model and the Numerical Methods. There are two established methods for determining the shape of a particle. It is known that the equilibrium shape of a crystal of fixed volume can usually be predicted by the Wulff construction,[12] which implies that the area of a particular surface is related to the surface energy. However, the Wulff construction is only valid for large particles (>10 nm).[13] For small metal clusters, when the number of atoms goes beyond 40, the potential energy surfaces become so complicated that global optimization becomes computationally very challenging.[14] In this work, we make an assumption based on TEM images[6] that the MCNPs of 2 nm in size are amorphous and are roughly spherical. Practically, we define three radii, and cut spherically from the bulk of α-Mo_2C (*Pbcn*) with a C atom at the center (Figure 1). The spherical

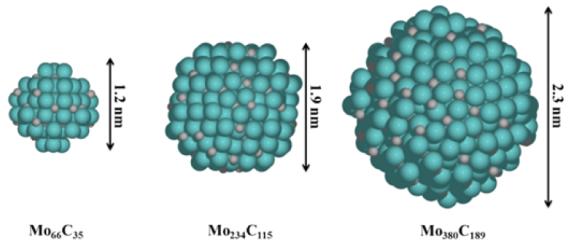

Figure 1. Original MCNPs cut spherically from the bulk Mo_2C without optimization; the Mo atoms are green and the C atoms are gray.

particles were then subjected to simulated annealing for a short time (7 ps, Δt = 0.1 fs), Born−Oppenheimer molecular dynamics (BOMD) (deMonNano[15]) heating to 673 K, followed by a local geometry optimization. 0.1 fs was used as the time step for both DFTB and the later DFTB/MM MD simulations for two reasons. There is an empirical equation for determining Δt in DFTB MD simulations:[16]

$$\Delta t = 0.25 \times \sqrt{m_{\min}/m_{\mathrm{H}}} \times \sqrt{300\ \mathrm{K}/\max(T_0,\ 5\ \mathrm{K})}$$

where $m_{\min}$ is the minimum atomic mass of the system and m_{H} is the mass of the hydrogen atom. This equation suggests a time step of 0.167 fs. Second, our later tests of 0.2 fs as the time step show that the system is unstable. The standard DFTB parameters (without SCC) developed in our previous work[17,18] were used for all DFTB calculations. UFF type dispersion[19] corrections are added to all systems, with the exception of the data in 3.1−3.6 (for comparison to the QM/MM data, for which the QM part does not have a dispersion term implemented).

Benzene molecules are then added to the selected sites of optimized MCNPs, followed by another geometry optimization. Since these medium-sized MCNPs are assumed to be amorphous, it is therefore very difficult to define "active sites" as we usually do in surface chemistry. However, previous cluster[4] and periodic[5] DFT calculations indicate that "Mo−Mo−Mo" 3-fold sites, where benzene interacts with three Mo atoms, are the most stable adsorption sites for benzene. Our previous periodic DFT calculations[5] also suggest Mo−Mo bridge sites, or 2-fold sites where benzene interacts with two Mo atoms, are also good for benzene adsorption. This has been confirmed by test calculations on the adsorption of benzene on the MCNPs using DFTB. In this work, we consider two types of active sites for benzene: 3-fold hollow sites, and 2-fold bridge sites. H_2 is assumed to adsorb dissociatively on the 3-fold hollow sites of the molybdenum carbide surface with high surface mobility, as previous DFT calculations[20] show. We follow the Horiuti−Polanyi mechanism,[21] and consider only the addition to the C atoms on the C_6 ring by the closest adsorbed H atoms. The decomposition of the H_2 molecule on the nanoparticle and the diffusion of the H atoms are beyond the scope of our current study. The attacking H atoms were introduced by adding them below the target C atom at a distance slightly larger than a C−H distance (usually 1.5 Å), followed by another geometry optimization.

The energies of the reacting species E_i' are calculated as

$$E_i' = E_i - E_{\mathrm{ref}}$$
$$E_{\mathrm{ref}} = E_{\mathrm{NP}} - E_{\mathrm{BEN}} - 3E_{\mathrm{H_2}}$$

where E_{NP}, E_{BEN}, and $E_{\mathrm{H_2}}$ are the energies of the nanoparticle, benzene and H_2 molecules in the gas phase, and

$$E_i = E_{\mathrm{sys}} + (3 - n)E_{\mathrm{H_2}}$$

$$\text{with } n = \begin{cases} 1 \text{ for 1st and 2nd hydrogenation} \\ 2 \text{ for 3rd and 4th hydrogenation} \\ 3 \text{ for 5th and 6th hydrogenation} \end{cases}$$

For thermal corrections, the Hessian matrix of the reactant states, transition state, and product states of the QM systems are calculated with DFTB+,[22] and the vibrational modes calculated with the Modes code, which is distributed along with DFTB+. The internal energy U and the free energy A are calculated with the ThermoAnalysis[23−25] code using the following equations:

$$U = E_{\mathrm{e}} + E_{\mathrm{t}}(T) + E_{\mathrm{r}}(T) + E_{\mathrm{v}}(T)$$
$$S = S_{\mathrm{e}} + S_{\mathrm{t}} + S_{\mathrm{r}} + S_{\mathrm{v}}$$
$$A = U - TS$$

where the subscript e, t, r, and v represent the electronic, translational, rotational, and vibrational contributions. We define $(E_{\mathrm{t}} + E_{\mathrm{r}} + E_{\mathrm{v}})$ as the thermal corrections to the electronic energy, and $(-TS)$ as the entropy correction to the internal energy with harmonic vibrational analysis. The temperatures for all the corrections are 673 K.

QM/MM Models and Numerical Methods. In the QM/MM potential, we used the additive self-consistent charge (SCC)-DFTB/CHARMM interface implemented by Cui et al.,[10] with total energy expression as follows:

$$E^{\mathrm{tot}} = \langle \Psi | \hat{H}^{\mathrm{QM}} + \hat{H}_{\mathrm{el}}^{\mathrm{QM/MM}} | \Psi \rangle + E_{\mathrm{van}}^{\mathrm{QM/MM}} + E^{\mathrm{MM}}$$

All MD simulations are performed with the CHARMM[26] code with time step of 0.1 fs. The dispersion corrections between QM atoms in the QM/MM calculations are neglected, because comparisons of NEB calculations with and without QM dispersion show only marginal differences. The van der Waals (VDW) interactions between QM and MM ($E_{\mathrm{van}}^{\mathrm{QM/MM}}$) are based on the UFF[27] VDW parameters. Improvements were made by using reference density functional theory (DFT) calculations with the GGA-PBE functional, DZVP/GEN-A2 basis and auxiliary set and dispersion corrections (see Supporting Information).

In order to study the six elementary hydrogenation reactions in solvent, we take the optimized reactant states of the six reactions from the 1.2 nm MCNP QM model, and still treat them quantum mechanically in QM/MM. These QM regions are then embedded separately into an environment of 100 benzene molecules, which are treated by molecular mechanics using the CHARMM force field. The systems were packed into spheres of 3 nm in diameter with Packmol[28] with a distance criterion of 2.0 Å. This ensures that the atoms from different molecules keep safe pairwise distances.

In all the following QM/MM geometry optimizations and MD simulations, a miscellaneous mean field potential (MMFP) spherical harmonic potential of 200 (kcal/mol)/Å is added to restrain the system into a sphere of 3 nm in diameter. The effectiveness of this boundary potential is manifested by the observation of little change in the volume of the system during the MD. The packed systems were then optimized for 500 steps with the steepest descent algorithm. Since the purpose of this optimization is to reduce the possibly large initial forces on the atoms, convergence has to be attained. 500 steps was sufficient for this purpose because the QM region is already optimized before embedding, and the relative configurations of the

DOI: 10.1021/jacs.5b01494
J. Am. Chem. Soc. 2015, 137, 4249−4259

MM benzene molecules are already optimized based on the GENCAN algorithm[29] in Packmol. It was observed that the total energy of the system remains in an interval of ±10 kcal/mol after 450 steps of optimization. As an example, the optimized embedded reactant state of the first hydrogenation reaction is shown in Figure 2.

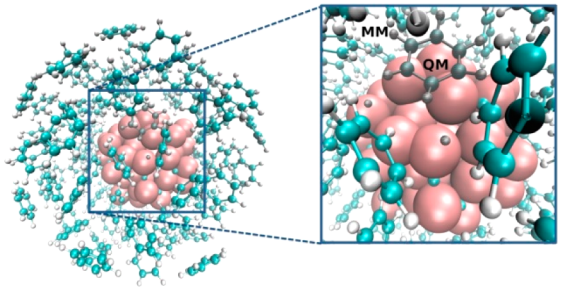

Figure 2. QM/MM model of a 1.2 nm MCNP (Mo atoms in red and C atoms in cyan) with adsorbed benzene (in black) and the two dissociated H atoms (in black) embedded in the model aromatic solvent.

To ensure sufficient sampling for each reaction, the QM regions of the optimized systems are temporarily constrained rigidly (CONS FIX in CHARMM), and the MM regions are subjected to 50, 100, and 200 ps of MD simulation to generate three different MM starting structures. Thus, for each of the six hydrogenation reactions, three different starting MM configurations are generated, which are named MM1, MM2, and MM3. For each of these MM configurations, the system is slowly heated up to 673 K again and equilibrated for 8 ps with a time step of 0.1 fs. Afterward, for each one of the three equilibration trajectories generated above, three configurations are randomly picked. This is done by using a random number generator to generate three numbers, and assign to each of the trajectories that belongs to the same hydrogenation reaction. These starting QMMM configurations are named as QMMM1, QMMM2, ..., QMMM9. Using these techniques, we are able to do umbrella sampling calculations using nine different starting configurations for each of the hydrogenation reactions.

For each umbrella sampling window, the system is first heated up to 673 K and equilibrated using the Gaussian velocity reassignment method (1.5 ps), and then subjected to 3.0 ps of Nose–Hoover dynamics (TREF = 673 K, QREF = 500, NCYC = 5) to ensure strict NVT ensembles. After the MD simulations, the biasing forces applying to the system by MMFP were recovered with the weighted histogram analysis method (WHAM) to get the PMF. The WHAM code from Prof. T. Allen[30] (2003) was used, and the convergence criteria for the free energies were set to 0.001 kcal/mol with a bin size of 0.01 Å. The ranges of the reaction coordinates to which WHAM was applied are listed in the Supporting Information. The first 2000 data points are skipped to avoid the initial disturbance caused by switching the temperature control method from Gaussian velocity reassignment to Nose–Hoover. To calculate the overall PMF, the windows with the same equilibrium reaction coordinate (z) from umbrella samplings with different starting configurations are combined, and then subjected to a WHAM analysis with the same parameters as indicated previously.

RESULTS AND DISCUSSION

1. Relaxed MCNPs. All of the MCNPs change from the ordered bulk structure to distorted structures after the simulated annealing (Figure 3). The magnitude of structural change depends on their sizes. The smaller 1.2 nm MCNP undergoes more change than the other larger ones. Besides the reorganization, there is also a little shrinking of the MCNPs, which is most obviously reflected by the largest 2.3 nm one.

One of the most important indicators of the electronic structure of catalysts is probably the band gap (for bulk systems) or the HOMO–LUMO gap (for molecules). The HOMO–LUMO gaps of the three MCNPs are calculated as shown in Table 1. It is usually believed that the smaller the nanoparticle, the larger the HOMO–LUMO orbital gap. As the size increases and HOMO and LUMO orbitals form the valence band and the conduction band, the gap narrows. The calculated HOMO–LUMO gaps of the MCNPs follow this trend. However, for transition metal clusters, the nonmetal to metal transition occurs at quite small cluster sizes, for example Ni at n = 16 and Pt at n = 60.[31] Considering the sizes of the three nanoparticles, they should have fairly small HOMO–LUMO gaps and the electronic structure change should not be very significant. Indeed, as Table 1 shows, all three nanoparticles have very small HOMO–LUMO gaps; they are all metallic. Since the HOMO–LUMO gap could be method dependent, we also tried the PM6 semiempirical method, but it was found that convergence could not be achieved with these amorphous MCNPs.

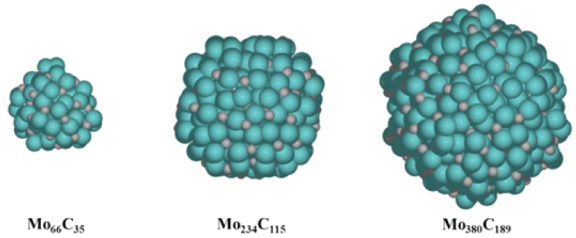

Figure 3. MCNPs subjected to simulated annealing; the Mo atoms are green and the C atoms are gray.

Table 1. DFTB HOMO-LUMO Gaps of the MCNPs

size of the MCNP (nm)	1.2	1.9	2.3
HOMO–LUMO gap (eV)	0.0047	0.0028	0.0012

2. Benzene Hydrogenation on Plain MCNPs in the Gas Phase. The calculated potential energy profiles of benzene hydrogenation on selected sites of the three MCNPs are shown in Figure 4. For both sites of the three MCNPs, most of the hydrogenation reactions are endothermic, and the overall exothermic nature of benzene hydrogenation on the transition metal catalysts is due to the release of energy from benzene and H_2 adsorption. This is consistent with benzene hydrogenation reactions on Pt[31] and Pd[32] from DFT calculations.

Following the Langmuir–Hinshelwood mechanism, the reactions start with the adsorption of benzene, and are followed by coadsorption of H_2 on the MCNPs (Figure 5b,c). For the adsorption of benzene and dissociative adsorption of H_2 on MCNPs, the choice of active sites is more important than that of the size of the nanoparticles. This is reflected by the relative closeness of the two 2-fold sites (black and green) curves and the 3-fold site curves (red and blue) in Figure 4. The 3-fold-sites are not as favorable as the 2-fold sites because in the benzene adsorption step too much energy has been released and benzene tends to bind very strongly with the catalyst. This makes the overall barrier higher than the 2-fold sites, and is in agreement with the idea of the Sabatier principle.

In all the five reaction path curves in Figure 4, the first hydrogenation reaction usually has a small barrier, while the second one has a higher barrier. There are two reasons for this. First, the aromaticity of benzene is broken upon adsorption, so the addition of the first hydrogen does not have to overcome a high barrier. Second, when the benzene is adsorbed, the

DOI: 10.1021/jacs.5b01494
J. Am. Chem. Soc. 2015, 137, 4249–4259

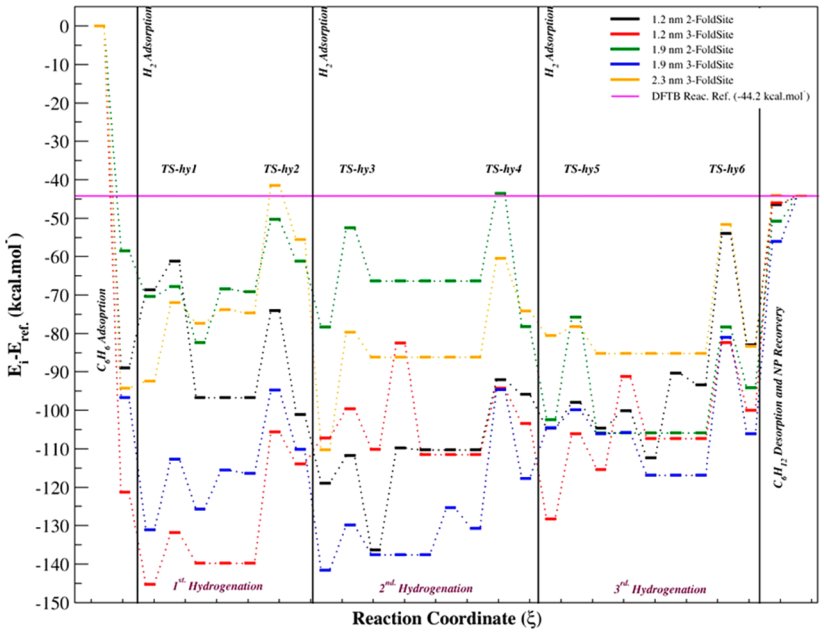

Figure 4. Potential energy profile ($E_i - E_{ref}$, where $E_{ref} = E_{NP} - E_{BEN} - 3E_{H_2}$) of benzene hydrogenation on different sites and sizes of MCNPs.

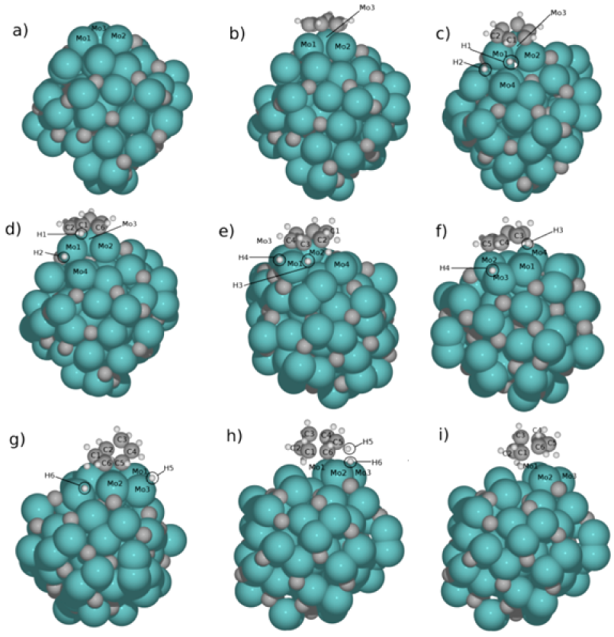

Figure 5. Optimized structures of the consecutive steps of benzene hydrogenation on a 3-fold site of the 1.2 nm MCNP.

distances between the C_6 ring and the catalyst surface is the lowest during the hydrogenation processes. On either a 3-fold site or a 2-fold site, there is always a C atom (C1 in Figure 5c) that is not interacting directly with any Mo atoms, but is very close to a 3-fold site that is made up of two Mo atoms on the first layer (Mo1 and Mo2 in Figure 5c) and a second layer Mo (Mo4 in Figure 5c). The initial H−C distance in this case is usually much smaller, making it more convenient for the first hydrogenation reaction to occur compared to other hydrogenation reactions.

Once the first H takes a good position and attacks a nondirect-binding C atom, the second hydrogen is left with direct-binding C atoms (C2 and C6 in Figure 5d). Also adsorbing on a 3-fold site, the second H usually is further away from the target direct-binding C atom (C2 in Figure 5d), typically further than 2.7 Å. The second H therefore has to "climb" around the Mo atom that interacts directly with the target C atom for the hydrogenation. For the third and fourth hydrogenation, although in most reaction paths studied, the two H atoms have a similar situation as the first and second H atoms, the C_6 ring usually undergoes readjustments such as rotation after the first and second hydrogenation, moving the target C atoms to various different locations. The 3-fold positions for H adsorption either no longer exist or they do not have the ideal position for hydrogenation, and as a result, other adsorption sites that are closer to the target C have to be used. For example in the third hydrogenation step on a 3-fold site of the 1.2 nm MCNP, the third and fourth H atoms are both on the top sites of Mo1 (Figure 5e). Later, for the fourth hydrogenation to happen, the fourth hydrogen has to travel from the Mo1 top site (Figure 5e) to the Mo3 top site (Figure 5f). All these factors come into play in the third and fourth hydrogenation, and make the potential energy profiles of these two elementary steps less ordered than the first and second hydrogenations.

After the first four hydrogenation reactions are finished, the C_6H_{10} molecule usually adsorbs on the MCNP such that the remaining two CH groups interact with one single Mo atom (Figure 5g). This state, upon the fifth hydrogenation, is changed to a state that has only one C atom interacting directly with the Mo atom, but with a closer distance, indicating a stronger C−Mo interaction. This enhancement of one C−Mo interaction compensated for the breaking of the other C−Mo interaction. This is reflected by the generally small barriers for the fifth hydrogenation. The last hydrogenation reactions in all the reaction paths have quite high and consistent barriers. This is because in all the reaction paths studied, the last hydrogen has to break similar C−Mo bonds between the C of the last CH group and the Mo atom that it is directly interacting with (Figure 5h), and forms cyclohexane, for which no direct C−Mo interaction exists anymore (Figure 5i).

In most of the studied benzene hydrogenation reaction paths, the additions of the second H to produce cyclohexadiene or the

DOI: 10.1021/jacs.5b01494
J. Am. Chem. Soc. 2015, 137, 4249−4259

sixth H to produce cyclohexane have the highest barriers among all the steps. At the end of the six hydrogenation reactions, we observed that the structure of the MCNP changed compared to the initial state before reaction. The MCNP thus has to have a "regeneration" step to close the catalytic cycle. Benzene hydrogenation on isolated MCNPs can be summarized as a catalytic cycle shown in Figure 6.

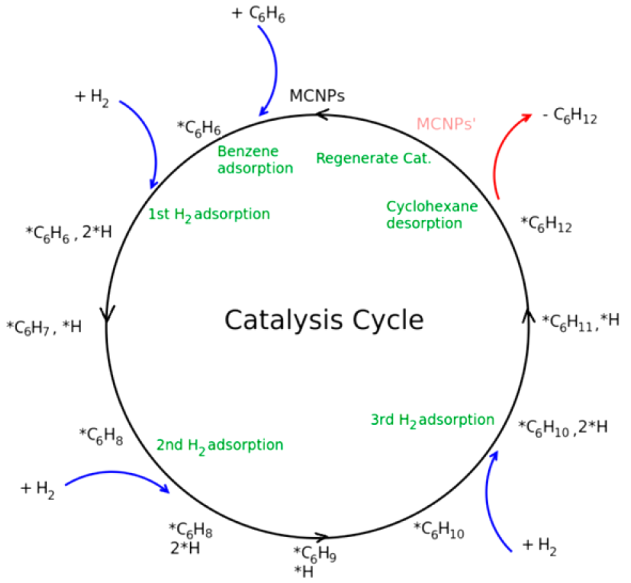

Figure 6. Horiuti–Polanyi type catalytic cycle of benzene hydrogenation on MCNPs.

At this point, we've successfully carried out studies following the traditional way of thinking in computational heterogeneous catalysis. However, this is not the end of the story. The main target of the work is to go beyond the traditional thinking, and find what was missing between the traditional way of modeling in heterogeneous catalysis and the reality in nature. Specifically, we would like to know how the solvent and the entropy of the system contribute to these nanoscale solid/liquid heterogeneous reactions.

In the next section, with the thermal corrections based on vibrational analysis, the above unsolvated reactions on the 1.2 nm MCNP will be compared to the corresponding solvated reactions from QM/MM umbrella sampling, to reveal more features of the reactions.

3. Benzene Hydrogenation on the 1.2 nm MCNP in the Model Aromatic Solvent. In this section, the degrees of freedom related to the Helmholtz free energy A (or PMF) of benzene hydrogenation reaction on the 1.2 nm MCNP from different starting configurations in QM/MM umbrella sampling are presented. The scope also includes the quantities from the traditional method of geometry optimization-NEB-MEP search + vibrational analysis and thermal correction. The electronic energy (E), subjected to thermal corrections for energy components, leads to the internal energy (U); the entropy corrections to the internal energy (U) with vibrational analysis gives the Helmholtz free energy (A). Focusing on the comparison among these quantities, and the comparison of the free energy from the QM system with vibrational analysis to the free energy (PMF) of the solvated system, the six hydrogenation reactions will be discussed one by one.

For each reaction, since the PMFs from different configurations are essentially describing the same state on the reaction coordinate, they can be combined into one overall PMF curve statistically with WHAM. We will use this overall PMF curve for our discussion. Among the individual PMF curves with different starting configurations, the differences in the absolute values of the free energies come from aligning the free energy fragments from the unbiased distributions of each window into one overall PMF curve in WHAM; therefore, they are purely numerical artifacts. For this reason, the PMF curves can be shifted up/down without changing their physical meaning. We present these individual PMF curves only to show the convergence of our umbrella sampling.

Since all of the quantities we are discussing are state functions, a reference state has to be defined. For the free energy, we define the lowest point on the overall-PMF as zero. For the potential energy, internal energy, and free energy curves of the QM system, we put them in such a way that the point corresponding to the reaction coordinate (z) of the reactant state matches with that of the overall PMF curve from QM/MM umbrella sampling. There are two reasons for this. First, this allows us to compare the shape and the barriers of the reaction profiles at different reaction coordinate in a more meaningful way. Second, this is a relatively well-defined state, as all the QM/MM umbrella samplings windows start with the configuration with the QM region similar to the reactant states of the QM calculations.

3.1. Addition of the First Hydrogen. Looking at the PMF curves from umbrella sampling with different starting configurations (the 9 dashed curves named as PMF-MMi-QMMMj in Figure 7), one can see that the PMF curves are

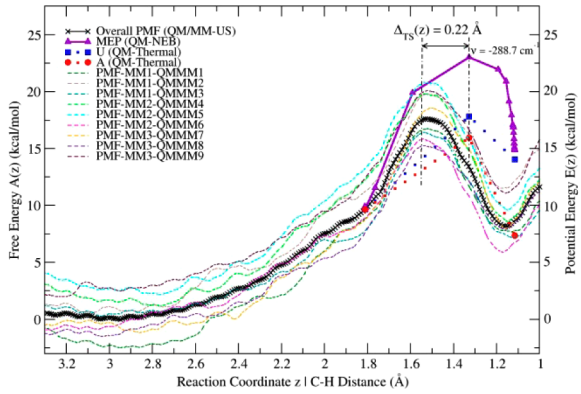

Figure 7. Calculated PMF of the first hydrogenation reactions from different starting configurations; "MM" means the MM configuration of the solvent benzene molecules; "QMMM" means the overall configuration of the whole system, including both the QM region and the MM region. U and A are calculated from the thermal analysis of the QM system on the minimum energy path (MEP).

largely parallel with one another. Considering that they are from different starting configurations in a random way, we can say that the umbrella sampling calculations have largely converged. Among the solvent configurations (MM1, MM2, and MM3), no clear difference can be found from the PMF curves of the umbrella samplings. Therefore, the exact configurations of the solvent molecules are not important for the reaction. The barriers of the individual PMF and the overall PMF for the first hydrogenation reaction are summarized in the Supporting Information.

DOI: 10.1021/jacs.5b01494
J. Am. Chem. Soc. 2015, 137, 4249–4259

Next, we focus on the overall PMF (the thick black curve made up of "×" symbols) obtained from combing all the sampled states. The C−H distance of the hydrogenation product state is 1.1−1.2 Å, similar to the value found on the MEP of the unsolvated MCNP. However, the initial reactant states are not the same between the two systems. On the MEP of the unsolvated reaction, a C−H distance of 1.8 Å was found for the reactant state. However, QM/MM umbrella sampling shows that this is a not a stable local minimum under working conditions. Because of the complexity of the surface of the MCNP, the movements of the Mo atom on the MCNP could easily lead to the change of the local topology of the active site for H adsorption. In other words, under working conditions, the active sites of the H adsorption positions on the MCNPs may form and disappear dynamically because of solvation and entropic effects.

As Table 2 shows, the thermal correction to the electronic energy ($E_t + E_r + E_v$) greatly lowered the ΔE barrier from 13.3 to 8.1 kcal/mol. Among the three terms, the vibrational contribution to the internal energy E_v is the dominant factor, which makes up over 99% of the correction. The entropy corrections (mostly from S_v) with the harmonic approximation not only further lowered the barrier to 6.3 kcal/mol, but also greatly stabilized the product state by 6.7 kcal/mol. Comparing the free energies obtained by QM-Thermal and QM/MM-US, there is a difference of 1.6 kcal/mol to the transition state, and a 2.0 kcal/mol difference in the product state. Also, there is a fairly large discrepancy between the shape of the free energy profile and the potential energy profiles, most obviously manifested by the difference in the transition state structures of the two methods (0.22 Å). These can be attributed to the contribution of the entropy of the system, including the solvent. Under working conditions, the entropy of the MCNP and the solvent molecules could affect the reaction during the entire course of the reaction coordinate. The approaching of the H atom to the target C atom causes the irreversible entropic relaxation of the MCNP and probably the solvent. Evidence suggesting the coupling of the movements of H atoms and Mo atoms during the hydrogenation is the low imaginary frequency (−288.7 cm^{-1}) of the transition state, resulting from the combination of the formation of a C−H bond and the bending of the benzene ring which changes the lengths of several Mo−C bonds.

Table 2. Relative Thermodynamic Quantities for the First Hydrogenation Reaction[a]

states	$E_{(QM\text{-}NEB)}$	$U_{(QM\text{-}Thermal)}$	$A_{(QM\text{-}Thermal)}$	$A'_{(QM/MM\text{-}US)}$	$A' - A$
$R_{QM\text{-}NEB}$	0.0	0.0	0.0	0.0	0.0
TS	13.3	8.1	6.3	7.9	1.6
P	5.2	4.4	−2.3	−0.3	2.0

[a]The reactant state from QM-NEB calculation defined as the reference state. "R" means reactant state with reaction coordinate (z) predicted by QM-NEB, "TS" means transition state, and "P" means product state; all units in kcal/mol.

3.2. Addition of the Second Hydrogen. For the addition of the second hydrogen, the QM geometry optimization and the QM/MM-US predicted similar reactant states with $z \approx 2.8$−2.9 Å. The hydrogenation process can be divided into two stages (Figure 8). In the range of z = (2.8 Å, 1.8 Å) when the H atom is at the early stage of approaching the target C atom, the traditional MEP from NEB has a much steeper shape than the PMF from umbrella sampling. However, in the range of z = (1.8 Å, 1.0 Å), the situation is the inverse, and MEP is less steep than PMF. The PMF obtained from umbrella sampling seems to "smooth out" the inflection points of the MEP. This difference in the shape of the MEP and PMF can be attributed to the entropic relaxation of the whole system (including the solvent) at the working temperature. Both methods predicted similar transition state structures with $z \approx 1.5$ Å. Visualization of the mode with the imaginary frequency of the transition state (−1244.8 cm^{-1}) shows that it involves the scissoring movement of the Mo−H bond with respect to the Mo−C bond, which ends up with the breaking of the Mo−H bond and the formation of a C−H bond.

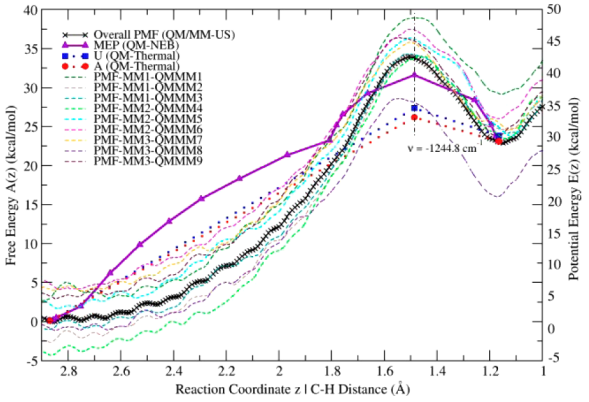

Figure 8. Calculated free energy profiles of the second hydrogenation reactions from different starting configurations. "MM" means the MM configuration of the solvent benzene molecules; "QMMM" means the overall configuration of the whole system, including both the QM region and the MM region.

As Table 3 shows, the thermal correction to the electronic energy (mostly from E_v) decreases the transition state energy by 4.2 kcal/mol, but has little effect on the product state (+0.7 kcal/mol). The same is true for the entropy correction (mostly from E_v) with the harmonic approximation, with −1.2 kcal/mol for the transition state, and −0.7 kcal/mol for the product state. Despite the fact that the transition state structures predicted by the two methods have similar (z) values (Figure 8), the free energies for the states are quite different, with +7.7 kcal/mol for the transition state, and +12.1 kcal/mol for the product state. This suggests that the anharmonic vibrational entropy of the nanoparticle and the entropy of the solvent make fairly large contributions to this reaction.

Table 3. Relative Thermodynamic Quantities for the Second Hydrogenation Reaction[a]

states	$E_{(QM\text{-}NEB)}$	$U_{(QM\text{-}Thermal)}$	$A_{(QM\text{-}Thermal)}$	$A'_{(QM/MM\text{-}US)}$	$A' - A$
$R_{QM\text{-}NEB}$	0.0	0.0	0.0	0.0	0.0
TS	31.5	27.3	26.1	33.8	7.7
P	23.0	23.7	23.0	10.9	12.1

[a]The reactant state from QM-NEB calculation defined as the reference state. "R" means reactant state with reaction coordinate (z) predicted by QM-NEB, "TS" means transition state, and "P" means product state; all units in kcal/mol.

3.3. Addition of the Third Hydrogen. For the addition of the third hydrogen, the overall PMF has a free energy barrier of 26.2 kcal/mol. Similar to the first hydrogenation reaction, the traditional geometry optimization predicted a reactant state far

DOI: 10.1021/jacs.5b01494
J. Am. Chem. Soc. 2015, 137, 4249−4259

from that obtained by QM/MM umbrella sampling (Figure 9). There is a difference of 0.8 Å for the reaction coordinate, and

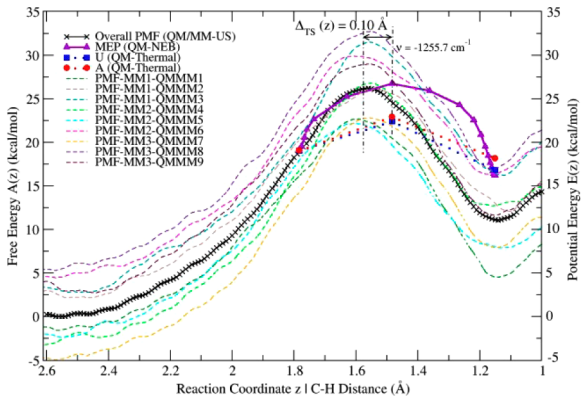

Figure 9. Calculated free energy profiles of the third hydrogenation reactions from different starting configurations. "MM" means the MM configuration of the solvent benzene molecules; "QMMM" means the overall configuration of the whole system, including both the QM region and the MM region.

almost 20 kcal/mol difference between the reactant state predicted by geometry optimization and QM/MM umbrella sampling. To rule out the possibility of a loose convergence criterion, the optimization convergence criterion for the force was reduced to 0.0001 eV/Å (or 3.67×10^{-7} Hartree/Å), but still yields a state very near with an energy decrease of only 0.016 kcal/mol. This suggests that at high temperature, this local minima obtained by geometry optimization may not exist, because of the entropic effect of the nanoparticles and the solvent. The irreversible entropic relaxation of the system may change the local topology of the nanoparticle, causing the H atoms to move from z = 1.8 Å to about 2.5 Å.

If we consider the approach of H from z = 1.8 to z = 1.15, the transition state has an imaginary frequency of −1255.7 cm^{-1}, showing the same type of scissoring motion of the Mo−H bond and a Mo−C bond as the second hydrogenation reaction. The reaction coordinate of the transition state is different by 0.10 Å between the two methods. Both methods predict a very small barrier of only a few kcal/mol, and the addition of the third hydrogen to be a fast reaction. This is in agreement with the high energy and unstable nature of the adsorbed reactant C_6H_8 from our previous DFT studies.[4] Considering the entire region of z = 2.4 Å to z = 1.2 Å, the free energy barriers of the reaction mostly come from the movement of the H atom from an unfavorable distance to a favorable position on the unordered surface of the MCNP in the solvent. This again proves our earlier judgment that the surface topologies of the MCNPs are very important for their catalytic activities.

As Table 4 shows, for this elementary reaction, the thermal corrections to the energy (mostly from E_v) lowered the potential energy barrier by 4.4 kcal/mol, but did not affect the product state very much (+0.7 kcal/mol). Inversely, the entropic correction (mostly from S_v) with the harmonic approximation made little contribution to the transition state (+0.6 kcal/mol), but affected the product state more (+1.3 kcal/mol). Comparing the free energies obtained by the two methods, the one from QM/MM-US is different from the thermal and harmonic entropy corrected one by 3.2 kcal/mol for the transition state, and −3.1 kcal/mol for the product state.

Table 4. Relative Thermodynamic Quantities for the Third Hydrogenation Reaction[a]

states	$E_{(QM\text{-}NEB)}$	$U_{(QM\text{-}Thermal)}$	$A_{(QM\text{-}Thermal)}$	$A'_{(QM/MM\text{-}US)}$	$A' - A$
$R_{QM\text{-}NEB}$	0.0	0.0	0.0	0.0	0.0
TS	7.7	3.3	3.9	7.1	3.2
P	−2.9	−2.2	−0.9	−4	−3.1

[a]The reactant state from QM-NEB calculation defined as the reference state. "R" means reactant state with reaction coordinate (z) predicted by QM-NEB, "TS" means transition state, and "P" means product state; all units in kcal/mol.

These differences can be attributed to the anharmonic vibrational entropy of the QM region and the solvent effect.

3.4. Addition of the Fourth Hydrogen. For the fourth hydrogenation, the PMF curves from different starting configurations are not as ordered as for the other reactions, although they are largely parallel with one another (Figure 10).

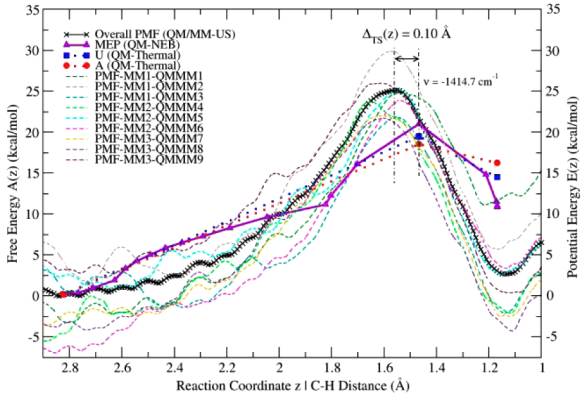

Figure 10. Calculated free energy profiles of the fourth hydrogenation reactions from different starting configurations. "MM" means the MM configuration of the solvent benzene molecules; "QMMM" means the overall configuration of the whole system, including both the QM region and the MM region.

The "bumpy" region of z = (2.9 Å, 1.8 Å) exists because the further the H atom is away from the target C atom, the less well-defined the system is. As we only constrained the C−H distance, the H atom could be in different situations for the constrained MD simulations with different starting configurations.

As Figure 10 shows, both methods predicted similar reactant state and product state in terms of the reaction coordinate with $z \approx 2.8$ Å. However, there is a difference of 0.10 Å between the reaction coordinates of the transition state from the two methods. The relatively small difference in $\Delta_{TS}z$ (similar to the third hydrogenation, but different from the first hydrogenation) is because of the small contribution from the movements other than the C−H vibration, as indicated by the frequency (−1414.7 cm^{-1}). In the vibrational mode of the imaginary frequency, a scissoring movement very similar to the second and third hydrogenations was found, except that in the fourth hydrogenation the target C atom is a little further away from the Mo. Therefore, when the H forms a C−H bond with the target C atom, one can only observe the tilting up of the other C−H bond (the one already existing), but there is not much change in the C−Mo distance. Since the C−Mo vibrational frequency is usually below 400 cm^{-1} (see ref 18), the imaginary frequency of the fourth hydrogenation is slightly higher than

DOI: 10.1021/jacs.5b01494
J. Am. Chem. Soc. 2015, 137, 4249−4259

that of the second (−1255.8 cm^{-1}) and third (−1244.7 cm^{-1}), because of the loss of the coupling with the C−Mo low frequency vibrations.

Thermal corrections (mostly from E_v) to the potential energy are relatively small for the transition state (−1.5 kcal/mol), but larger for the product state (+3.7 kcal/mol) (Table 5). The entropy correction (mostly from S_v) with the harmonic approximation also contributed −0.9 kcal/mol and +1.7 kcal/mol to the free energies of the transition state and the product state. Despite these corrections, there is still quite a large difference between the free energies calculated with the two methods: 6.5 kcal/mol for the transition state, and 6.2 kcal/mol for the product state, because of the anharmonic vibrational entropy of the QM region and the solvent effect.

Table 5. Relative Thermodynamic Quantities for the Fourth Hydrogenation Reaction[a]

states	$E_{(QM\text{-}NEB)}$	$U_{(QM\text{-}Thermal)}$	$A_{(QM\text{-}Thermal)}$	$A'_{(QM/MM\text{-}US)}$	$A' - A$
$R_{QM\text{-}NEB}$	0.0	0.0	0.0	0.0	0.0
TS	20.8	19.3	18.4	24.9	6.5
P	10.7	14.4	16.1	22.3	6.2

[a]The reactant state from QM-NEB calculation defined as the reference state. "R" means reactant state with reaction coordinate (z) predicted by QM-NEB, "TS" means transition state, and "P" means product state; all units in kcal/mol.

3.5. Addition of the Fifth Hydrogen. For the fifth hydrogenation, both methods predict similar transition state structures with z = 2.7−2.8 Å (Figure 11). This reaction is similar to the second and the fourth hydrogenation in many respects. In the fifth hydrogenation, the MEP from NEB also shows two distinct regions. In the region of z = (2.8 Å, 1.8 Å), the MEP is almost linear, while the PMF is a smooth bent curve. In the other region of z = (1.8 Å, 1.1 Å), they have a similar curvature. There is also a difference of 0.10 Å in the reaction coordinate of the transition state between the two methods. The fifth hydrogenation is especially similar to the fourth one in the sense that they have very close transition states as indicated by the imaginary frequencies. This is because the target C atom in the fifth hydrogenation is also far away from the Mo atoms, which leads to an imaginary frequency of −1490.1 cm^{-1}, using the same reasoning as in the previous section.

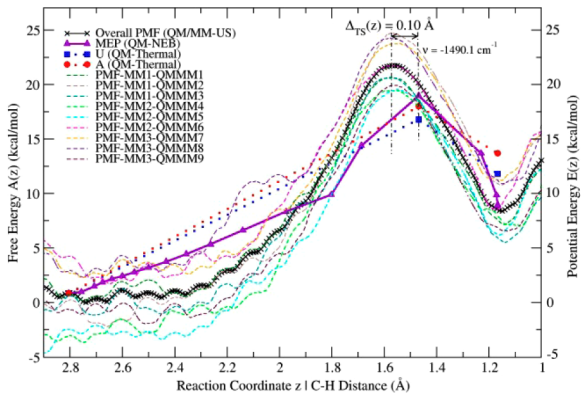

Figure 11. Calculated free energy profiles of the fifth hydrogenation reactions from different starting configurations. "MM" means the MM configuration of the solvent benzene molecules; "QMMM" means the overall configuration of the whole system, including both the QM region and the MM region.

As Table 6 shows, thermal corrections (mostly from E_v) to the potential energy correspond to −2.2 kcal/mol to the transition state and +2.9 kcal/mol to the product state. The entropy correction (mostly from S_v) with the harmonic approximation contributed +1.2 kcal/mol and +1.9 kcal/mol to the transition state and the product state, respectively. Comparing the free energies obtained with the different methods, they are very similar on the product state (differ by −0.4 kcal/mol), but differ more in the transition state (differ by +3.7 kcal/mol).

Table 6. Relative Thermodynamic Quantities for the Fifth Hydrogenation Reaction[a]

states	$E_{(QM\text{-}NEB)}$	$U_{(QM\text{-}Thermal)}$	$A_{(QM\text{-}Thermal)}$	$A'_{(QM/MM\text{-}US)}$	$A' - A$
$R_{QM\text{-}NEB}$	0.0	0.0	0.0	0.0	0.0
TS	18.1	15.9	17.1	20.8	3.7
P	8.0	10.9	12.8	12.4	−0.4

[a]The reactant state from QM-NEB calculation defined as the reference state. "R" means reactant state with reaction coordinate (z) predicted by QM-NEB, "TS" means transition state, and "P" means product state; all units in kcal/mol.

3.6. Addition of the Sixth Hydrogen. For the sixth hydrogenation, the PMF curves are also "bumpy" from 2.5 to 1.9 Å, but become smooth from 1.9 to 1.0 Å, although there is also a little disturbance close to the product state at $z \approx 1.1$ Å (Figure 12). The reaction coordinate of the initial reactant states are not exactly the same between the two methods, with a difference of about 0.2 Å. However, what is most significant is the difference in the shape of the MEP and the PMF, and the reaction coordinates of the transition states from them ($\Delta_{TS}z$ = 0.23 Å). The MEP curve is obtuse, while the PMF has a much sharper shape. The imaginary frequency (−197.3 cm^{-1}) of the transition state is similar to the first hydrogenation, but much lower than the other hydrogenation reactions. The vibrational mode of this imaginary frequency shows that the addition of the sixth hydrogen mostly involves the breaking of a C−Mo bond, i.e., the bond formed by the only CH carbon left and the corresponding Mo atom. Most of the energy is used to lift the

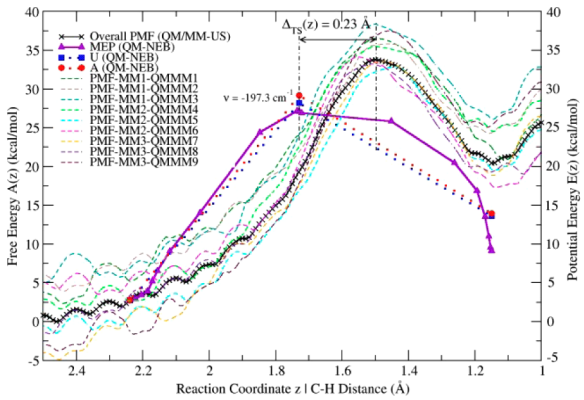

Figure 12. Calculated free energy profiles of the sixth hydrogenation reactions from different starting configurations. "MM" means the MM configuration of the solvent benzene molecules; "QMMM" means the overall configuration of the whole system, including both the QM region and the MM region.

DOI: 10.1021/jacs.5b01494
J. Am. Chem. Soc. 2015, 137, 4249−4259

last C atom from the MCNP surface; the attachment of the H atom and the formation of the C−H bond then happen favorably. Because of the great involvement of the C and Mo atoms for this reaction and the first hydrogenation, the entropy of the system (including the solvent) has a huge effect on the calculated free energy profiles and the transition state structures.

The thermal correction (mostly from E_v) to the potential energy is small for the transition state of this reaction (+1.0 kcal/mol) compared to its contribution to the product state (4.5 kcal/mol) (see Table 7). The entropy correction (mostly from S_v) with the harmonic approximation is small for both the transition state (+1.0 kcal/mol) and the product state (−0.7 kcal/mol). However, the anharmonic vibrational entropy of the nanoparticle and the entropy of the solvent contributed to the free energies by +4.6 kcal/mol to the transition state, and −0.7 kcal/mol to the product state.

Table 7. Relative Thermodynamic Quantities for the Sixth Hydrogenation Reaction[a]

states	$E_{(\text{QM-NEB})}$	$U_{(\text{QM-Thermal})}$	$A_{(\text{QM-Thermal})}$	$A'_{(\text{QM/MM-US})}$	$A' - A$
$R_{\text{QM-NEB}}$	0.0	0.0	0.0	0.0	0.0
TS	24.4	25.4	26.4	31.0	4.6
P	6.3	10.8	11.2	10.5	−0.7

[a]The reactant state from QM-NEB calculation defined as the reference state. "R" means reactant state with reaction coordinate (z) predicted by QM-NEB, "TS" means transition state, and "P" means product state; all units in kcal/mol.

4. Entropic Effects and Nanoscale Heterogeneous Reactions in Solvent. In an environment that is similar to its working conditions, the 1.2 nm MCNP shows some different features from that of the unsolvated MCNP. Among them, the most interesting one is the observation of the contribution from the anharmonic vibrational entropy of the nanoparticle and the entropy of the solvent in the course of the reactions. They could change the shape (steepness) of the reaction path, modify the free energy barriers, and affect the initial state and the transition state structures of the hydrogenation reactions on MCNPs. In particular, the more the reaction process is related to the movement of the MCNP (the first and the sixth hydrogenation reactions), the more significant the changes of the transition states. These observations make us wonder why this phenomenon could happen.

Let us take one step back, and first think about the plain transition metal nanoparticles without surface reactants or the solvent. For transition metal nanoparticles of metallic nature, the electrons are highly delocalized, and there are many possible bonding/electronic configurations, which leads to the easy change among the geometric configurations (isomers), especially for the surface atoms that have higher degrees of freedom than those in the interior of the particle. Li et al.[33] imaged the same Au_N nanoparticles (where $N = 309 \pm 6$) in several successive frames, and found that their structures change at room temperature. The first direct observation of the surface-only fluxionality was recently reported by Sun et al, who found that small Ag (<10 nm) nanoparticles, with high bulk melting point of 962 °C, behave like liquid droplet on the surface and deform easily even at room temperature (300 K),[34] while keeping crystalline cores. The deformation of these transition metal nanoparticles are essentially entropic effects, which can only be observed in situ.[34] These findings imply that the entropic effect is an indispensable consideration for transition metal nanoparticles even at room temperature.

What would happen if chemical reactions are to occur on these transition metal nanoparticles at high temperature, in other words, transition metal nanocatalysts? The simulations we've performed in this work are for the in situ benzene hydrogenation reactions on MCNPs in solvent. It is known that molybdenum carbide is highly metallic,[35] and the band near the Fermi level (0−1 eV) is mostly composed of Mo 4d orbitals.[36] As we've found earlier, the MCNPs as small as 1.2 nm are also highly metallic. When surface reactions happen, during the course of the reaction, the movement of the surface species causes irreversible deformations of the nanoparticles on the reaction paths, which is observed as the entropy of the system (including the solvent), and reflected in the difference in the potential energy profiles and the free energy profiles of our computational simulations. The entropic effect manifests itself by the strong motion of the MCNPs at high temperature (673 K) as benzene hydrogenation takes place on the catalyst, and the motions are patently not harmonic (repetitive in time) vibrations. (See Video S1 and Video S2 in the Supporting Information.)

One should not, however, confuse the energetic structural change of the MCNP during the hydrogenation reactions (reflected by the "regeneration" step in the catalytic cycle) with the deformation of the MCNP due to the entropic effect. The former is an energetic effect that is included in the MEP from NEB. The latter, however, is found in the difference between the MEP and the PMF, and is mostly entropic.

So far, there is no direct experimental data on the kinetics of benzene hydrogenation on MCNPs. Future experimental study is needed to validate the findings in this work. Despite the advantages of the current QM/MM-US method, there are several aspects that may require attention for future improvements, and will be discussed here. First, DFTB is a semiempirical QM method, which has lower accuracy than ab initio or first-principles methods. Replacing DFTB with a QM method of higher accuracy is suggested, to the extent permitted by computational power.

Second, because of the light mass of hydrogen, nuclear quantum effects could be important for the reactions that involve hydrogen transfer, such as catalytic hydrogenation reactions. Hydrogen transfer is a well-known reaction in biochemistry in which the nuclear quantum effect is evident.[37−40] As Klinman et al. have found,[38] quantum tunneling is driven by thermal vibrations of the enzyme; pure tunneling has been established as a possible mechanism for the enzymic breakage of C−H without ascending the barrier. However, understanding how quantum effects impact the reactivity of hydrogen in heterogeneous catalysis is at a very early stage. McIntosh et al.[41] investigated tunneling assisted surface diffusion of hydrogen on Ru(0001) with DFT path-integral molecular dynamics (PIMD) and quantum transition state theory (QTST).[42] The quantum effect reduced the classical free energy barrier of hydrogen diffusion on Ru(0001) by 35% at very low temperature (70 K) by the tunnel effect, but only slightly (10%) reduced the barrier when the temperature is high (250 K) because of the zero point energy (ZPE) effect, with a crossover temperature of about ∼120 K from tunneling-dominated diffusion to classical diffusion. Similarly, a low temperature tunneling effect was observed for hydrogen diffusion on Ni(111), but through excited vibrational states.[43] Because of the relatively high temperature of the in situ catalysis

DOI: 10.1021/jacs.5b01494
J. Am. Chem. Soc. 2015, 137, 4249−4259

environment (673 K), nuclear quantum effect of hydrogen motion on MCNP should not be very significant.

Third, the sand particles that the MCNPs may be adsorbed on could potentially affect the electronic structure as well as the translational, rotational, and vibrational degrees of freedom of the MCNPs. Therefore, the sand particles could have both energetic and entropic effects on the free energy barriers and the rates of the hydrogenation reactions. Thus, the sand particles in the oil reservoir should be added to the system for future studies.

CONCLUSIONS

In this work, benzene hydrogenation on MCNPs in the gas phase and in a model aromatic solvent was investigated. Electronic structure calculations with DFTB show that all the three MCNPs are highly metallic with similar HOMO−LUMO gaps. In the size range of the MCNPs tested, surface topology plays a more important role in determining the catalytic activity of the active sites. In particular, 2-fold sites are more favorable, because of smaller benzene adsorption energy, which leads to lower overall potential energy barriers, in agreement with the empirical Sabatier principle.[44] Among the six elementary reactions, the addition of the second or the last hydrogen usually has the highest barrier. During the hydrogenation reactions, the MCNPs had slight changes in structure, and must have a regeneration step to complete the catalytic cycle, although molybdenum carbide is known for its high hardness. The six hydrogenation reactions of benzene on the MCNP can be quite different from one another. For example on the 1.2 nm MCNP, the first and the sixth hydrogenation reactions involve a lot of C−Mo motion, while the second, third, fourth, and fifth hydrogenation reactions mostly happen with the scissoring motions of the Mo−H bond with respect to the Mo−C bond. Because of the strong dependence on the topology of the nanocatalysts, it has been proposed[45,46] earlier that no generalized mechanism for the catalytic reaction on small nanoparticles can be given.

To simulate the reaction in a more realistic manner, and to account for the temperature, pressure, and the solvent environment of the system, a QM/MM model was built, and the umbrella sampling approach was used to calculate the PMF of the reaction. The data are compared to the traditional approach in computational heterogeneous catalysis, i.e., geometry optimization, transition state search on the potential energy surfaces, and thermal and entropy corrections based on the harmonic approximation. We found from our calculations that the transition metal nanocatalysts are very "flexible", rather than being rigid in their working conditions. A large part of this "flexibility" comes from the anharmonic vibrational entropy of the nanoparticle and the entropy of the solvent. It is for this reason that the entropic effect must be properly taken care of for the study of chemical reactions catalyzed by transition metal nanoparticles, preferably by sampling methods rather than simple thermal corrections which ignore anharmonic contributions. Also, more effort is needed in dealing with the environment and the entropic effects, besides improving the accuracy of the quantum mechanical methods for nanoscale heterogeneous catalysis reactions.

The advantages of multiscale modeling, specifically the QM/MM umbrella sampling method, in studying nanoscale solid/liquid heterogeneous catalysis reactions are demonstrated. Although limited by the current computational power and the accuracy of the available semiempirical algorithms, it can potentially be a very useful tool in understanding the features of nanoscale heterogeneous catalytic reactions. Future work will include the sand component into the multiscale model to simulate the in situ heavy oil catalysis system more realistically.

ASSOCIATED CONTENT

Supporting Information

The detailed parameters for umbrella sampling and the validation of the QM van der Waals parameters for the QM atoms are provided. Also included are the barriers of the individual PMF and the overall PMF for all the six hydrogenation reactions. This material is available free of charge via the Internet at http://pubs.acs.org.

AUTHOR INFORMATION

Corresponding Author

*dennis.salahub@ucalgary.ca

Notes

The authors declare no competing financial interest.

ACKNOWLEDGMENTS

We thank Dr. Pedro Pereira Almao and his group at the University of Calgary for useful discussions on the in situ oil sand upgrading processes. We also thank Dr. Thomas Heine at Jacobs University for helping developing the DFTB parameters and Dr. Mauricio Chagas da Silva for providing the code for thermal analysis. Lastly, we would like to thank NSERC for the funding and Compute Canada/Westgrid for providing the computational resources.

REFERENCES

(1) Frauwallner, M. L.; Lopez-Linares, F.; Lara-Romero, J.; Scott, C. E.; Ali, V.; Hernandez, E.; Pereira-Almao, P. *Appl. Catal., A* **2011**, *394*, 62.
(2) Hashemi, R.; Nassar, N. N.; Pereira-Almao, P. *Energy Fuels* **2013**, *27*, 2194.
(3) Pereira-Almao, P. *Can. J. Chem. Eng.* **2012**, *90*, 320.
(4) Liu, X.; Tkalych, A.; Zhou, B.; Köster, A. M.; Salahub, D. R. *J. Phys. Chem. C* **2013**, *117*, 7069.
(5) Zhou, B.; Liu, X.; Cuervo, J.; Salahub, D. R. *Struct. Chem.* **2012**, *23*, 1459.
(6) Hyeon, T. H.; Fang, M. M.; Suslick, K. S. *J. Am. Chem. Soc.* **1996**, *118*, 5492.
(7) Koskinen, P.; Mäkinen, V. *Comput. Mater. Sci.* **2009**, *47*, 237.
(8) Seifert, G.; Porezag, D.; Frauenheim, T. *Int. J. Quantum Chem.* **1996**, *58*, 185.
(9) Elstner, M.; Porezag, D.; Jungnickel, G.; Elsner, J.; Haugk, M.; Frauenheim, T.; Suhai, S.; Seifert, G. *Phys. Rev. B: Condens. Matter Mater. Phys.* **1998**, *58*, 7260.
(10) Cui, Q.; Elstner, M.; Kaxiras, E.; Frauenheim, T.; Karplus, M. *J. Phys. Chem. B* **2000**, *105*, 569.
(11) Roux, B. *Comput. Phys. Commun.* **1995**, *91*, 275.
(12) Wulff, G. *Z. Kristallogr.* **1901**, *34*, 449.
(13) Marks, L. D. *Surf. Sci.* **1985**, *150*, 358.
(14) Heiles, S.; Johnston, R. L. *Int. J. Quantum Chem.* **2013**, *113*, 2091.
(15) Heine, T; Rapacioli, M.; Patchkovskii, S.; Frenzel, J.; Köster, A. M.; Calaminici, P.; Escalante, S.; Duarte, H. A.; Flores-Moreno, R.; Geudtner, G.; Goursot, A.; Reveles, J. U.; Vela, A. Salahub, D. R. *deMonNano*; Jacobs University: Bremen, Germany, 2009.
(16) Heine T.; Rapacioli M.; Patchkovskii, S.; Frenzel, J.; Köster, A. M.; Calaminici, P.; Escalante, S.; Duarte, H. A.; Flores-Moreno, R.; Goursot, A.; Reveles, Salahub, D. R.; Vela, A. *The deMonNano Users' Guide [Online]*; Jacobs University: Bremen, Germany, 2009; p 72,

DOI: 10.1021/jacs.5b01494
J. Am. Chem. Soc. 2015, 137, 4249−4259

http://physics.jacobs-university.de/theine/research/deMon/deMonNano-nosrc.tgz (accessed Mar 1, 2013).
(17) Wahiduzzaman, M.; Oliveira, A. F.; Philipsen, P.; Zhechkov, L.; van Lenthe, E.; Witek, H. A.; Heine, T. *J. Chem. Theory Comput.* **2013**, *9*, 4006.
(18) Liu, X.; Wahiduzzaman, M.; Heine, T.; Salahub, D. R. *J. Chem. Theory Comput.* **2015**, to be submitted for publication.
(19) Zhechkov, L.; Heine, T.; Patchkovskii, S.; Seifert, G.; Duarte, H. A. *J. Chem. Theory Comput.* **2005**, *1*, 841.
(20) Ren, J.; Huo, C.-F.; Wang, J.; Cao, Z.; Li, Y.-W.; Jiao, H. *Surf. Sci.* **2006**, *600*, 2329.
(21) Horiuti, I.; Polanyi, M. *Trans. Faraday Soc.* **1934**, *30*, 1164.
(22) Aradi, B.; Hourahine, B.; Frauenheim, T. *J. Phys. Chem. A* **2007**, *111*, 5678.
(23) Silva, M. C. d. *ThermalAnalysis*, version 1.0;. Department of Chemistry, Federal University of Minas Gerais: Belo Horizonte, Brazil, 2012.
(24) Hill, T. L. *An Introduction to Statistical Thermodynamics*; Dover Publications: New York, 1960.
(25) McQuarrie, D. A.; Simon, J. D. *Molecular Thermodynamics*; University Science Books: Sausalito, CA, 1999.
(26) Brooks, B. R.; Brooks, C. L.; Mackerell, A. D.; Nilsson, L.; Petrella, R. J.; Roux, B.; Won, Y.; Archontis, G.; Bartels, C.; Boresch, S.; Caflisch, A.; Caves, L.; Cui, Q.; Dinner, A. R.; Feig, M.; Fischer, S.; Gao, J.; Hodoscek, M.; Im, W.; Kuczera, K.; Lazaridis, T.; Ma, J.; Ovchinnikov, V.; Paci, E.; Pastor, R. W.; Post, C. B.; Pu, J. Z.; Schaefer, M.; Tidor, B.; Venable, R. M.; Woodcock, H. L.; Wu, X.; Yang, W.; York, D. M.; Karplus, M. *J. Comput. Chem.* **2009**, *30*, 1545.
(27) Rappe, A. K.; Casewit, C. J.; Colwell, K. S.; Goddard, W. A.; Skiff, W. M. *J. Am. Chem. Soc.* **1992**, *114*, 10024.
(28) Martínez, L.; Andrade, R.; Birgin, E. G.; Martínez, J. M. *J. Comput. Chem.* **2009**, *30*, 2157.
(29) Dennis, J. E.; Schnabel, R. B. Numerical Methods for Unconstrained Optimization and Nonlinear Equations. *Classics in Applied Mathematics*; Society for Industrial & Applied Math: Philadelphia, PA, 1996; Vol. *16*.
(30) Allen, T. W.; Baştuğ, T.; Kuyucak, S.; Chung, S.-H. *Biophys. J.* **2003**, *84*, 2159.
(31) Sattler, K. In *Handbook of Thin Films*; Nalwa, H. S., Ed.; Academic Press: Burlington, MA, 2002; p 61.
(32) Saeys, M.; Reyniers, M. F.; Neurock, M.; Marin, G. B. *J. Phys. Chem. B* **2005**, *109*, 2064.
(33) Morin, C.; Simon, D.; Sautet, P. *Surf. Sci.* **2006**, *600*, 1339.
(34) Li, Z. Y.; Young, N. P.; Di Vece, M.; Palomba, S.; Palmer, R. E.; Bleloch, A. L.; Curley, B. C.; Johnston, R. L.; Jiang, J.; Yuan, J. *Nature* **2008**, *451*, 46.
(35) Sun, J.; He, L.; Lo, Y.-C.; Xu, T.; Bi, H.; Sun, L.; Zhang, Z.; Mao, S. X.; Li, J. *Nat. Mater.* **2014**, *13*, 1007.
(36) Politi, J. R. d. S.; Vines, F.; Rodriguez, J. A.; Illas, F. *Phys. Chem. Chem. Phys.* **2013**, *15*, 12617.
(37) Sugihara, M.; Ozawa, K.; Edamoto, K.; Otani, S. *Solid State Commun.* **2004**, *131*, 245.
(38) Cha, Y.; Murray, C.; Klinman, J. *Science* **1989**, *243*, 1325.
(39) Klinman, J. P. *Biochim. Biophys. Acta, Bioenerg.* **2006**, *1757*, 981.
(40) Klinman, J. P.; Kohen, A. *Annu. Rev. Biochem.* **2013**, *82*, 471.
(41) Bruno, W. J.; Bialek, W. *Biophys. J.* **1992**, *63*, 689.
(42) McIntosh, E. M.; Wikfeldt, K. T.; Ellis, J.; Michaelides, A.; Allison, W. *J. Phys. Chem. Lett.* **2013**, *4*, 1565.
(43) Voth, G. A.; Chandler, D.; Miller, W. H. *J. Chem. Phys.* **1989**, *91*, 7749.
(44) Badescu, S. C.; Ying, S. C.; Ala-Nissila, T. *Phys. Rev. Lett.* **2001**, *86*, 5092.
(45) Rothenberg, G. In *Catalysis*; Wiley-VCH Verlag GmbH & Co. KGaA: Weinheim, Germany, 2008; p 39.
(46) Arenz, M.; Landman, U.; Heiz, U. *ChemPhysChem* **2006**, *7*, 1871.

DOI: 10.1021/jacs.5b01494
J. Am. Chem. Soc. 2015, 137, 4249−4259